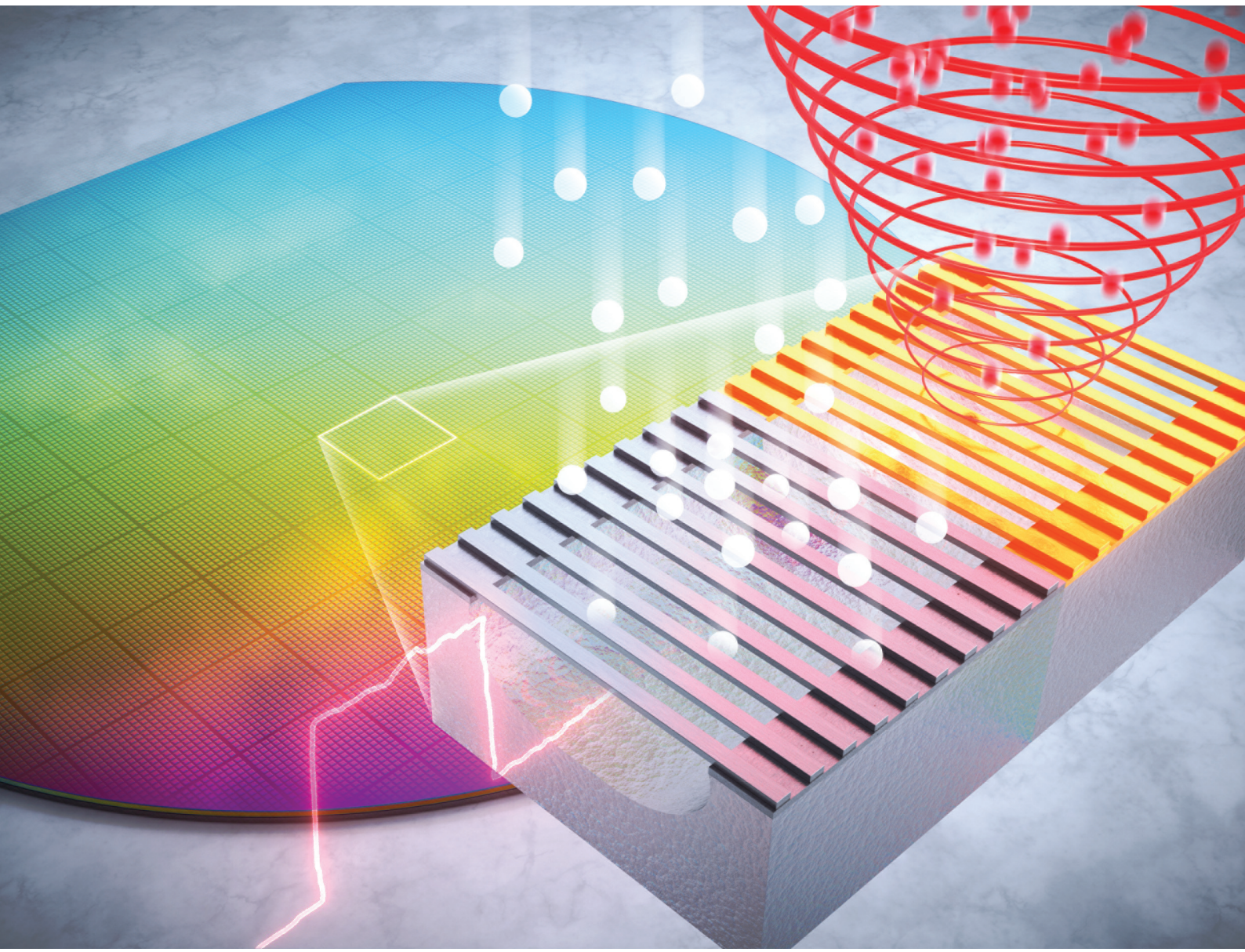
Volume 14
Number 4
28 January 2022
Pages 1021-1522

Nanoscale

rsc.li/nanoscale



ISSN 2040-3372

ROYAL SOCIETY OF CHEMISTRY

COMMUNICATION

Inkyu Park, Jun-Ho Jeong *et al.*

Wafer-scale, highly uniform, and well-arrayed suspended nanostructures for enhancing the performance of electronic devices

NCNST

Published on 30 December 2021. Downloaded by Korea Advanced Institute of Science & Technology / KAIST on 11/21/2022 2:00:33 PM.

Nanoscale

ROYAL SOCIETY OF CHEMISTRY

COMMUNICATION

View Article Online
View Journal | View Issue

Check for updates

Cite this: *Nanoscale*, 2022, **14**, 1136

Received 8th November 2021,
Accepted 22nd December 2021

DOI: 10.1039/d1nr07375c

rsc.li/nanoscale

Wafer-scale, highly uniform, and well-arrayed suspended nanostructures for enhancing the performance of electronic devices†

Zhi-Jun Zhao,‡[a] Junseong Ahn, ‡[b,c] Dongheon Lee,[d] Chan Bae Jeong,[e] Mingu Kang,[c] Jungrak Choi,[c] Moonjeong Bok,[b] Soonhyoung Hwang,[b] Sohee Jeon,[b] Sooyeon Park,[d] Jiwoo Ko,[b,c] Ki Soo Chang,[e] Jung-Woo Choi,[d] Inkyu Park *[c] and Jun-Ho Jeong *[b]

Suspended nanostructures play an important role in enhancing the performance of a diverse group of nanodevices. However, realizing a good arrangement and suspension for nanostructures of various shapes remains a significant challenge. Herein, a rapid and simple method for fabricating wafer-scale, highly uniform, well-arrayed suspended nanostructures *via* nanowelding lithography is reported. Suspended nanostructures with various shapes (nanowires, nanoholes, nanomesh, and nanofilms) and materials (gold, silver, and palladium metals) were employed to demonstrate the applicability of our method. Moreover, gas sensors and thermoacoustic speakers with suspended nanowires outperformed those with unsuspended nanostructures. The proposed method is expected to help advance the development of future nanodevices based on suspended nanostructures.

Introduction

Nanostructures with unique physical properties and functionalities have been widely applied in various devices, such as gas sensors,[1–7] photodetectors,[8] metalenses,[9] nanogenerators,[10] and biosensors.[11–13] Typically, nanostructures are directly fabricated on substrates using various methods[14–19] (*e.g.*, photolithography, e-beam lithography, nanoimprint lithography, spray, dip coating, and evaporation). However, owing to the direct contact between the bottom of the nanostructures and the substrate surface, the functionality of nanostructures cannot be maximized in applications that require higher surface-to-volume ratios, such as gas sensors[20] and thermoacoustic speakers.[21] Therefore, many types of suspended nanostructures have been developed and applied in various fields,[22–24] with good results. To date, most studies have reported that randomly suspended nanostructures enhance the surface-to-volume ratio and thereby improve the device performance. For example, suspended carbon nanotubes,[25] tungsten nanowires,[26] carbon nanowires,[27] and GaN nanowires[28] have been utilized to enhance the performance of gas sensors. Thermoacoustic speakers based on suspended graphene nanofilms,[29] carbon nanotubes,[30] and silver nanowires[31] have been widely reported, and they outperform those based on unsuspended nanostructures. However, the randomly suspended nanostructures could hinder the large-scale manufacturing of high-performance devices because of the uncontrollability of the structural design and complex fabrication processes. Recently, Yoon *et al.*[32,33] proposed a new nanowire platform to realize a 2D planar array of perfectly aligned, suspended nanowires, with good performance for heater and gas sensor applications. Their platform can help effectively fabricate of well-arrayed suspended nanowires. However, the complexity and cost of the process involving KrF lithography, xenon difluoride (XeF_2) etching, and oblique-angled depositions could bring some limitations for large-area fabrication and mass production as follows: (1) non-reusability of the nanograting fabricated *via* KrF lithography; (2) possible damage of suspended nanostructures by using XeF_2 etching gas, thereby the limiting the choice of material from which suspended nanostructures are made; (3) the complexity of repeated oblique-angled depositions process.

To address these issues, we propose a rapid and simple method for fabricating wafer-scale, highly uniform, well-arrayed suspended nanostructures *via* nanowelding lithogra-

[a]*Institute of Smart City and Intelligent Transportation, Southwest Jiaotong University, No. 999 Pidu District, Chengdu, Sichuan, China*
[b]*Department of Nano Manufacturing Technology, Korea Institute of Machinery and Materials (KIMM), Daejeon 34103, Republic of Korea. E-mail: jhjeong@kimm.re.kr*
[c]*Department of Mechanical Engineering, Korea Advanced Institute of Science and Technology (KAIST), Daejeon 34141, Republic of Korea. E-mail: inkyu@kaist.ac.kr*
[d]*School of Electrical Engineering, Korea Advanced Institute of Science and Technology (KAIST), Daejeon 34141, Republic of Korea*
[e]*Center for Scientific Instrumentation, Korea Basic Science Institute (KBSI), Daejon 34133, Republic of Korea*

† Electronic supplementary information (ESI) available: Additional SEM images, FIB images, optical images, and video of thermoacoustic speakers. See DOI: 10.1039/d1nr07375c

‡ These authors contributed equally.

This journal is © The Royal Society of Chemistry 2022

Published on 30 December 2021. Downloaded by Korea Advanced Institute of Science & Technology / KAIST on 11/21/2022 2:00:33 PM.

phy. Various nanostructures, including nanowires, nanoholes, nanomesh, and nanofilms, were easily and quickly welded onto the surface of a substrate prepared with "bridge piers" in 3 min, thereby forming perfectly suspended nanostructures. Moreover, various noble metals (*e.g.*, gold, silver, and palladium) were employed to fabricate well-arrayed suspended nanowires to demonstrate the wide applicability of the proposed method. We discuss how to achieve well-arrayed suspended nanostructures by analyzing the relationship between the bridge pier distance and the width of the suspended nanowires. Finally, a gas sensor and a thermoacoustic speaker with suspended nanostructures were fabricated; they outperformed devices with unsuspended structures.

Experimental

Si master and polymer mold preparation

Si masters with various nanostructures (*e.g.*, nanowires with widths of 200, 400, and 600 nm and pitch values of 400, 600, and 600 nm; nanoholes with a diameter of 750 nm and a pitch of 1500 nm; nanomesh with a side of 600 nm and a width of 200 nm) were prepared by KrF lithography. The prepared Si master can be used repeatedly to fabricate a polymer mold. RM-311 (Minuta Technology Co. Ltd, Korea, polyurethane) resin was used to fabricate the polymer mold.

Nanowelding lithography

The "bridge piers" with Au microstructures were fabricated *via* conventional photolithography, evaporation, lift-off, and reactive ion etching (RIE) (see Fig. 1a-6). Cr with the thickness of 3 nm was deposited to improve the adhesion force between Au and substrate. The fabricated nanostructures (Fig. 1a-5) were placed on the "bridge piers" *via* nanowelding process performed for a duration of 3 min at 160 °C under 3 bar pressure. After cooling for 1 min, the detachment process was implemented, thereby welding the nanostructure onto the surface of "bridge piers" owing to strong adhesion.[34,35]

Characterization

The surface morphologies and cross sections of the suspended nanostructures were observed using energy dispersive spectroscopy-field emission scanning electron microscopy (EDS-SEM, Sirion, FEI Netherlands) and a focused ion beam system (FIB, Helios Nanolab, FEI Netherlands), respectively.

Hydrogen gas sensor

An H_2 gas sensing test was conducted using a customized gas chamber, and the gas concentration was controlled using a

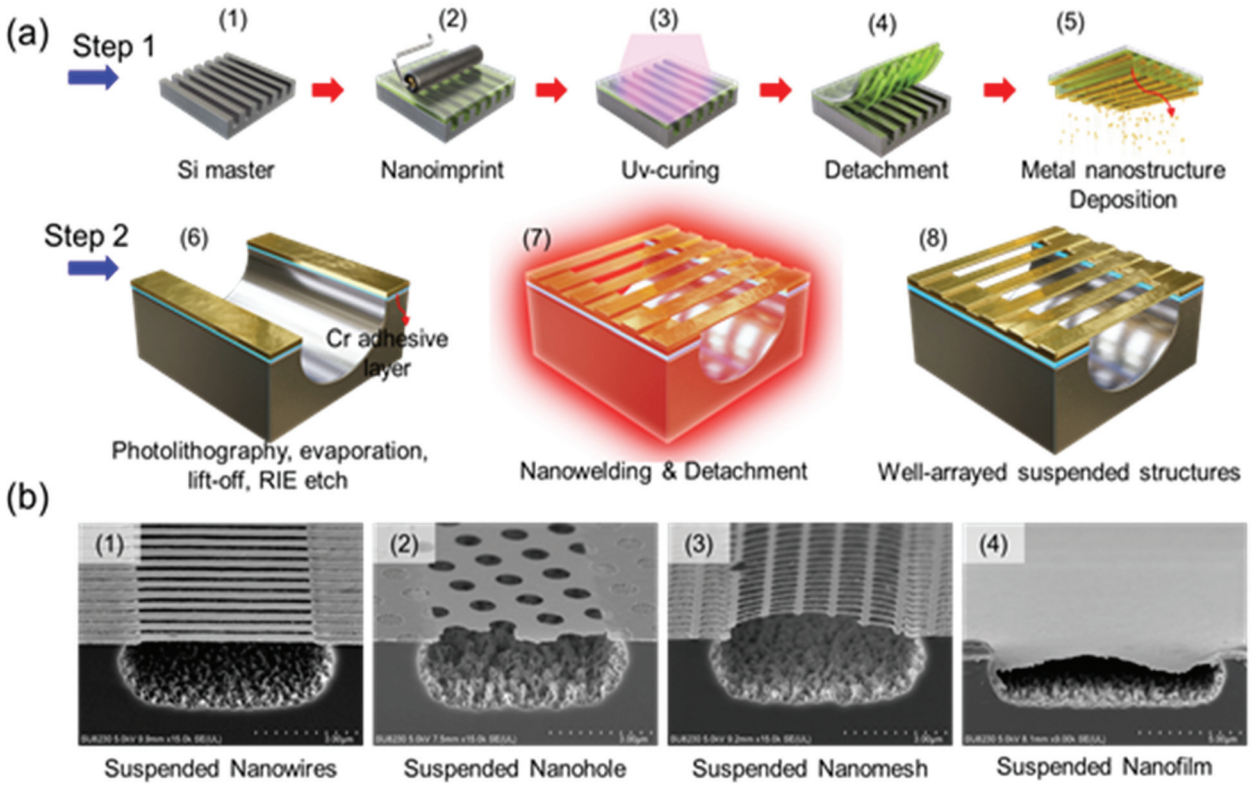


Fig. 1 Fabrication process and SEM images of well-arrayed suspended nanostructures: (a) fabrication process; (1)–(4) replication of polymer mold *via* nanoimprint, (5) deposition of metal nanostructure, (6) fabrication of Si wafer substrate with "bridge piers" using photolithography and dry etching, (7) nanowelding lithography, (8) completed well-arrayed suspended nanostructures. (b) SEM images of the suspended nanostructures with various shapes; (1) nanowire, (2) nanohole, (3) nanomesh, and (4) nanofilm.

Published on 30 December 2021. Downloaded by Korea Advanced Institute of Science & Technology / KAIST on 11/21/2022 2:00:33 PM.

mass flow controller. To prepare a specific concentration (0.4%, 0.8%, 1.2%, and 1.6%) of the H_2 gas, we supplied H_2, O_2, and N_2 gases with similar ratios as the ambient air to the gas chamber. During the gas test, the electrical resistance of the gas sensor was measured using a sourcemeter (2635 B, Keithley Instruments, USA). For the gas selectivity test, the concentration values of each tested gas were set close to the permissible exposure limit or lower explosive limit according to the safety guidelines (toxic and hazardous substances 1915.1000) defined by occupational safety and health administration (OSHA).[36]

Thermoacoustic speaker

To measure the heat distribution on the thermoacoustic speaker, an input voltage of 1.5 V was applied using a sourcemeter (2612 B, Keithley, USA), and the heat distribution was measured using customized thermoreflectance microscopy, which was developed in our previous work.[37,38] To investigate the sound pressure level of the thermoacoustic speaker, a sound input signal with a specific frequency and an applied power of 1 W was applied to the speaker using an audio analyzer (Clio FW-01, Audiomatica, Italy) and audio amplifier (QCBOX Model 5, Audiomatica, Italy). The sound output by the speaker was measured using a commercialized microphone (MIC-01, Audiomatica, Italy), and the signal was analyzed using an audio analyzer (Clio FW-01, Audiomatica, Italy) after amplification using a pre-amplifier (ANDIAMO.MC, Synthax, UK). The analyzed signal was monitored by a computer. All the aforementioned processes are described in Fig. 4c. To play the classical songs, a digital stereo amplifier (NA-DAMP3, NEOTICS, Republic of Korea) was connected to the developed speaker, and the sound signal was transmitted from a computer.

Results and discussion

Fig. 1a shows the fabrication process of the suspended nanostructures, which can be divided into two steps. In Step 1, metal nanostructures are obtained *via* e-beam evaporation. First, a Si master with the designed nanostructures is prepared (Fig. 1a-1). Second, a resin is coated onto the prepared Si master and then covered by polyethylene terephthalate (PET); thus, the resin is fully infiltrated into the Si master *via* rolling (Fig. 1a-2). Third, the UV curing process is implemented to achieve full polymerization (Fig. 1a-3). Fourth, the polymer mold with the designed nanostructures can be obtained by the detachment process (Fig. 1a-4). It should be noted that the polymer mold can be repeatedly replicated from the Si master, demonstrating the possibility of mass production. Finally, the designed metal nanostructures can be formed *via* vacuum deposition methods (Fig. 1a-5). In Step 2, well-arrayed suspended structures are fabricated *via* nanowelding lithography. First, the substrate with "bridge piers" is prepared *via* conventional photolithography, evaporation, lift-off, and RIE (Fig. 1a-6). "Bridge piers" can be easily designed depending on the application requirements. As an adhesive layer, Cr can enhance the adhesion force between the substrate and the metal structures. Second, the fabricated metal nanostructures (Fig. 1a-5) are welded onto the surface of the prepared "bridge piers" on the substrate (Fig. 1a-7) under a pressure of 3 bar, temperature of 160 °C, and for a duration of 3 min using nanowelding lithography, yielding well-arrayed suspended nanostructures (Fig. 1a-8). Fig. 1b shows the tilted SEM images of the suspended nanostructures fabricated by nanowelding lithography. Fig. 1b-1, b-2, b-3, and b-4 show the well-arrayed suspended Au nanowires, nanoholes, nanomesh, and nanofilms, respectively. To clearly observe the welding point between the "bridge piers" and nanostructures, focused ion beam (FIB) cross-sectional images are shown in Fig. S1.† To evaluate the mechanical stability of the suspended nanostructures, the suspended nanowires were chosen to observe the change in the nanowires depending on the size. Fig. 2a shows a variety of suspended nanowires depending on the distance between the "two bridge piers" and the nanowire width. A schematic of the suspended nanowires is shown in Fig. 2a-1, where D is the distance between the two bridge Piers and W is the nanowire width. In this work, suspended nanowires were fabricated with D values of 5, 10, and 20 μm and W values of 200, 400, and 600 nm.

Fig. 2a-2 shows the SEM images of the suspended nanowires with W of 200 nm and D of 5, 10, and 20 μm. When the nanowire width is 200 nm, we observe that as D increases, the suspended nanowires begin to deform under the effect of the contact stress and self-load, consistent with previous reports.[32,33] When W is 600 nm, the nanowires are perfectly fabricated on the "bridge piers" at distances of 5, 10, and 20 μm. This is because the larger width of the nanowires could improve the stiffness to resist the bending moment (in-plane bending and out-of-plane bending), thereby preventing deformation of the suspended nanowires and fracture due to mechanical stress. Fig. S2† shows the SEM images of the suspended nanowires when W is 400 nm and Fig. S3† shows large-scale images, which illustrate the uniformity of the suspended nanowires. From Fig. 2a, we find that the suspended structures can be easily fabricated using nanowelding lithography by adjusting the values of D and W. Notably, most conventional fabrication methods for the suspended or undercut nanostructure are based on wet or plasma etching processes; the substrate is etched after the deposition of the target materials on the patterned substrate. However, as the feature size of the devices shrinks, the surface tension of the liquid etchants begins to have deleterious effects on device yield, and the implantation of ions during plasma etching begins to impair the devices by changing the electrical characteristics or accumulating the mechanical stress.[39] We overcame these problems by attaching the nanostructures with the pre-fabricated "bridge piers" using nanowelding process, by which no additional mechanical or electrical damages occur on the suspended nanostructures.

To demonstrate the applicability of our method, various metals, including Pd, Au, and Ag, were chosen to fabricate the suspended nanowires with W = 200 nm and D = 5 μm. Fig. 2b-

 This journal is © The Royal Society of Chemistry 2022

Published on 30 December 2021. Downloaded by Korea Advanced Institute of Science & Technology / KAIST on 11/21/2022 2:00:33 PM.

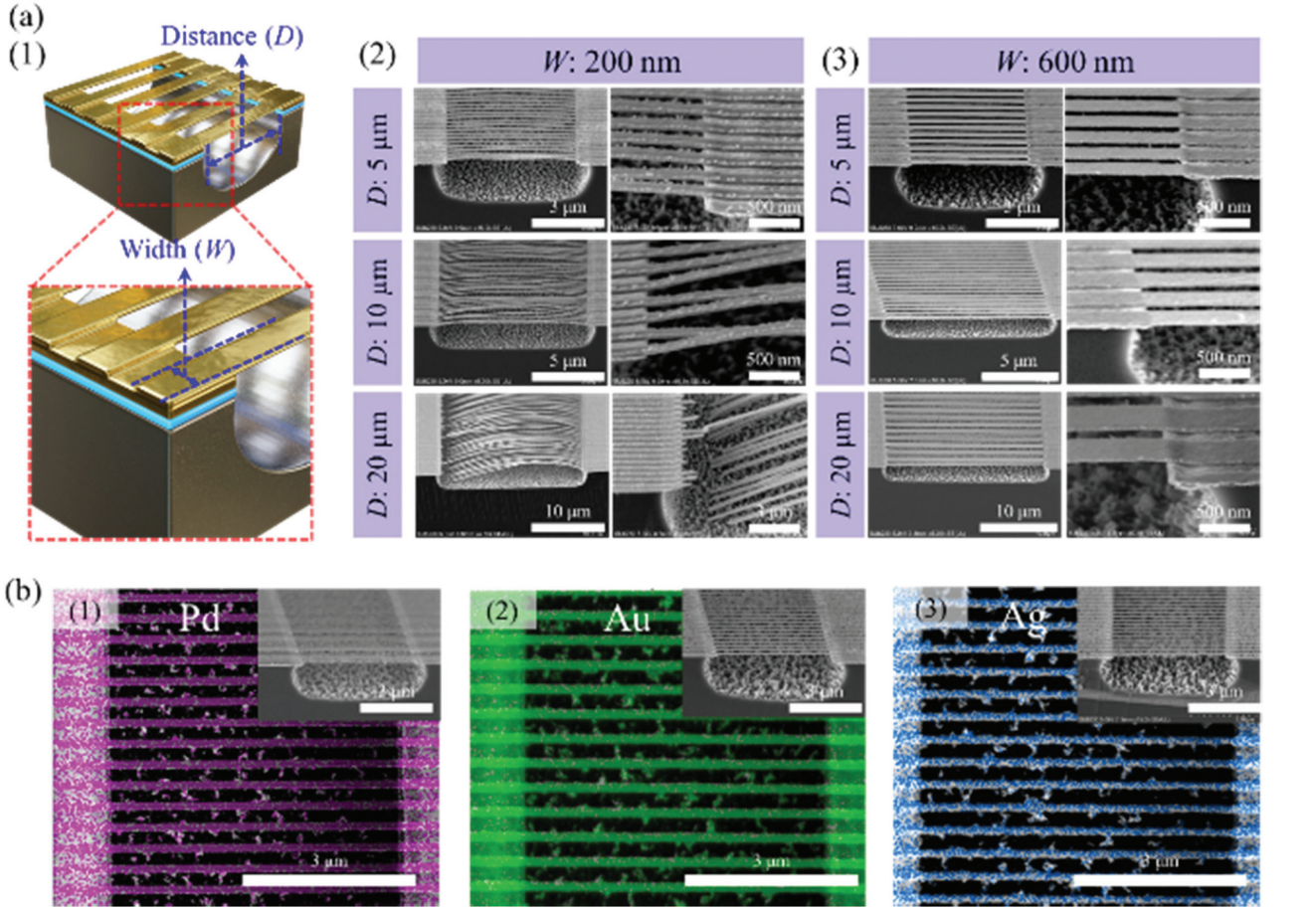


Fig. 2 Mechanical stability and applicability of suspended nanostructures. (a) Various suspended nanowires with different width (*W*) of the nanowires and distance (*D*) between "bridge Piers;" (1) Schematic of suspended nanowires, (2) SEM images of suspended nanowires with *W* of 200 nm and *D* values of 5, 10, and 20 μm, (3) SEM images of suspended nanowires with *W* of 600 nm and *D* values of 5, 10, and 20 μm. (b) EDS mapping and tilted SEM images of suspended nanowires with various metals (1) Pd, (2) Au, and (3) Ag.

1–b-3 show the related EDS mapping images. The inset images show the tilted SEM images of the suspended nanowires.

To verify the negligible influence of the substrate and utility of the suspended nanostructure, a Pd-based hydrogen (H_2) gas sensor is demonstrated as a promising application. Pd is attracting much attention as a sensing material for H_2 gas sensors because it is converted to palladium hydride (PdH_x) by absorbing H_2 gas under normal temperature and pressure conditions. In addition, the Pd-based gas sensors exhibit superior selectivity to H_2 gas and fast response, and can be driven at room temperature. Thus, they are considered the most promising H_2 gas sensors to satisfy the sensor performance targets set by US Department of Energy.[40] When Pd is exposed to H_2 gas, an electrical resistance change and mechanical deformation (volume expansion) occur. Therefore, to efficiently utilize these characteristics, various Pd-based H_2 gas-sensing structures have been developed.[41,42] In particular, nanostructured Pd-based H_2 gas sensors have a fast response and high sensitivity because of their high surface area-to-volume ratio (SA : V). However, most of the nanostructured Pd-based H_2 gas sensors developed so far are attached to supporting substrates, such as Si wafers or polymer films; therefore, the merits of nanostructuring have not been fully utilized.[43] That is, for a bound nanostructure, the effective SA : V is relatively low because the part attached to the substrate is not exposed to the target gas, and the amount of hydrogen absorption on Pd also decreases because of the mechanical constraints induced by the substrate. Recently, there have been many attempts to solve these problems, but only partially and randomly suspended nanowires[44] or a single nanowire[45] could be demonstrated because of the difficulty in fabricating fully suspended and well-arrayed nanostructures. Therefore, the developed fabrication method for well-arrayed suspended nanostructures was utilized to fabricate a hydrogen gas sensor to overcome the above-mentioned limitations.

Fig. 3a and b show the schematics and SEM images of the conventional surface-bound Pd nanowire-based gas sensor (B-GS) and the suspended Pd nanowire-based gas sensor (S-GS), respectively. Fig. S4† shows the optical microscopy and SEM images of the entire gas sensor, including the electrodes. In the case of B-GS, when the H_2 gas molecules are absorbed onto Pd, the substrate restricts the expansion of Pd and pre-

Published on 30 December 2021. Downloaded by Korea Advanced Institute of Science & Technology / KAIST on 11/21/2022 2:00:33 PM.

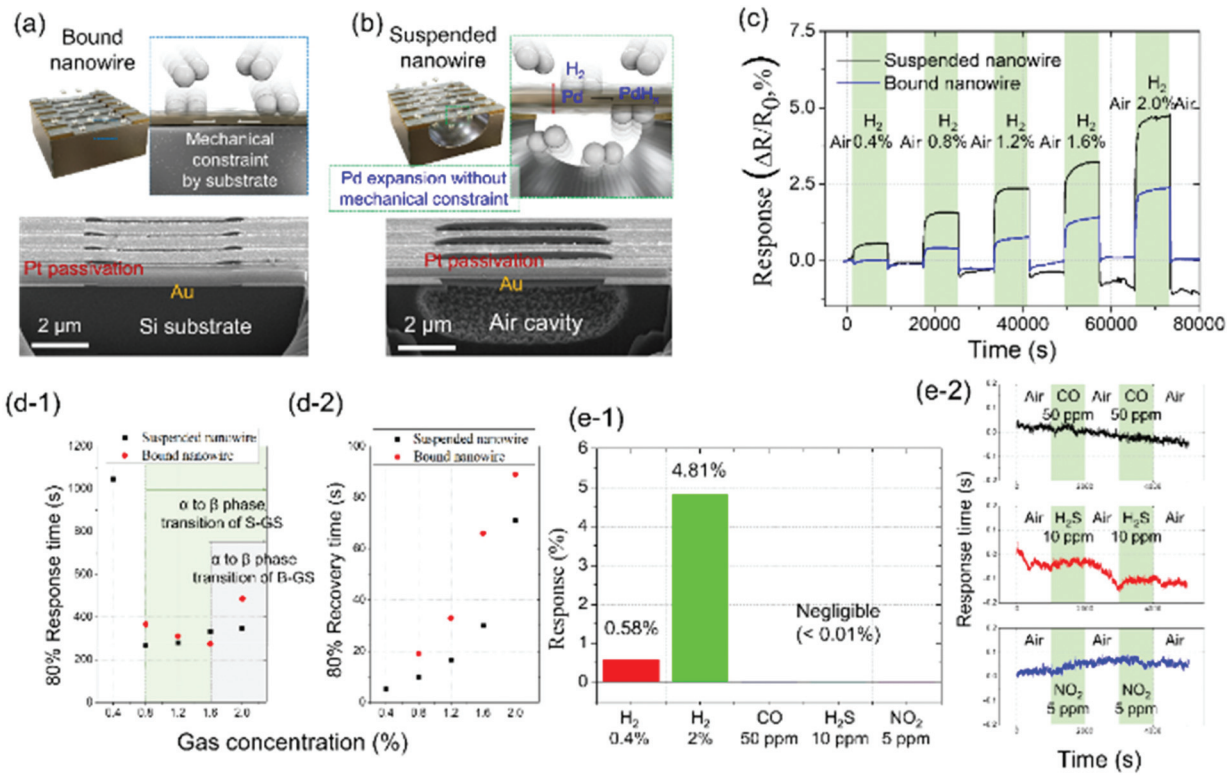


Fig. 3 Application of the suspended nanostructure to a hydrogen (H_2) gas sensor. (i) Schematic and (ii) cross-sectional SEM image of (a) bound Pd nanowire-based gas sensor (B-GS) and (b) suspended Pd nanowire-based gas sensor (S-GS). (c) Time-variant response of the gas sensors at different H_2 gas concentrations. (d-1) Response time and (d-2) recovery time of S-GS depending on the gas concentration. (e) Gas selectivity test of S-GS for 0.4% H_2, 2% H_2, CO, H_2S, and NO_2 gases: (e-1) summarized results and (e-2) raw response data for each gas.

vents Pd from fully reacting with the H_2 gas. On the other hand, in the case of S-GS, the gas molecules react on all four sides of the Pd nanowires, and most of the Pd can be converted to PdH_x without any substrate constraint. Therefore, S-GS can detect 0.4% H_2 gas, which cannot be detected by B-GS, and the sensitivity of S-GS is 2.01 times higher than that of B-GS at high concentrations of H_2 gas (2%), as shown in Fig. 3c. Fig. 3d shows the response and recovery times for each concentration. In general, the response time of Pd to H_2 gas decreases as the H_2 concentration increases; however, because the α-to-β phase transition of Pd occurs in approximately 0.8% to 2% H_2 gas, the response time increases as the hydrogen concentration increases in that region.[46] As shown in Fig. 3d–i, the response time of S-GS decreases as the H_2 concentration increases at low concentration of the H_2 gas (0.4–0.8% of H_2 gas) and increases thereafter, which coincides with the tendency of the response time of a suspended Pd single nanowire in a previously reported paper.[47] The response time of B-GS decreases in the range of 0.4% to 1.6% H_2 gas and thereafter increases. We suppose that the α-to-β phase transition of B-GS occurred at a higher H_2 gas concentration than that of S-GS owing to the substrate constraint. On the other hand, the recovery time of S-GS was shorter than that of B-GS across the entire concentration range. This is because the H_2 gas absorbed onto S-GS releases faster than that on B-GS regardless of the Pd phase because S-GS has a higher effective SA : V. Finally, the gas selectivity of the suggested S-GS was investigated, as shown in Fig. 3e. S-GS showed responses of 0.58% and 4.81% for 0.4% H_2 gas and 2% H_2 gas, respectively, while a negligible response (<0.01%) was observed for 50 ppm CO, 10 ppm H_2S, and 5 ppm NO_2 gases. The concentrations of each tested gas were set close to the permissible exposure limit or lower explosive limit defined by the OSHA.

A thermoacoustic speaker is another promising application to verify the effectiveness of the suspended nanostructures. As shown in Fig. 4a and b, the thermoacoustic speaker is based on the occurrence of time-dependent temperature variation by Joule heating when an AC voltage is applied to a conductor. The generated temperature variation causes the gas molecules in the ambient air to undergo mechanical vibration, which induces a sound pressure. The performance of the thermoacoustic speaker is not only affected by the heat capacity per unit area and the thermal effusivity of the conductor, but also by the heat dissipation due to the substrate.[48] Therefore, many studies are being conducted to minimize the thermal energy dissipated to the substrate by thermal conduction, and the best solution to date has been air insulation (suspended structure).[49,50] Because the developed fabrication process can rapidly produce large-area suspended nanostructures, it was used for fabricating thermoacoustic speakers.

 This journal is © The Royal Society of Chemistry 2022

Published on 30 December 2021. Downloaded by Korea Advanced Institute of Science & Technology / KAIST on 11/21/2022 2:00:33 PM.

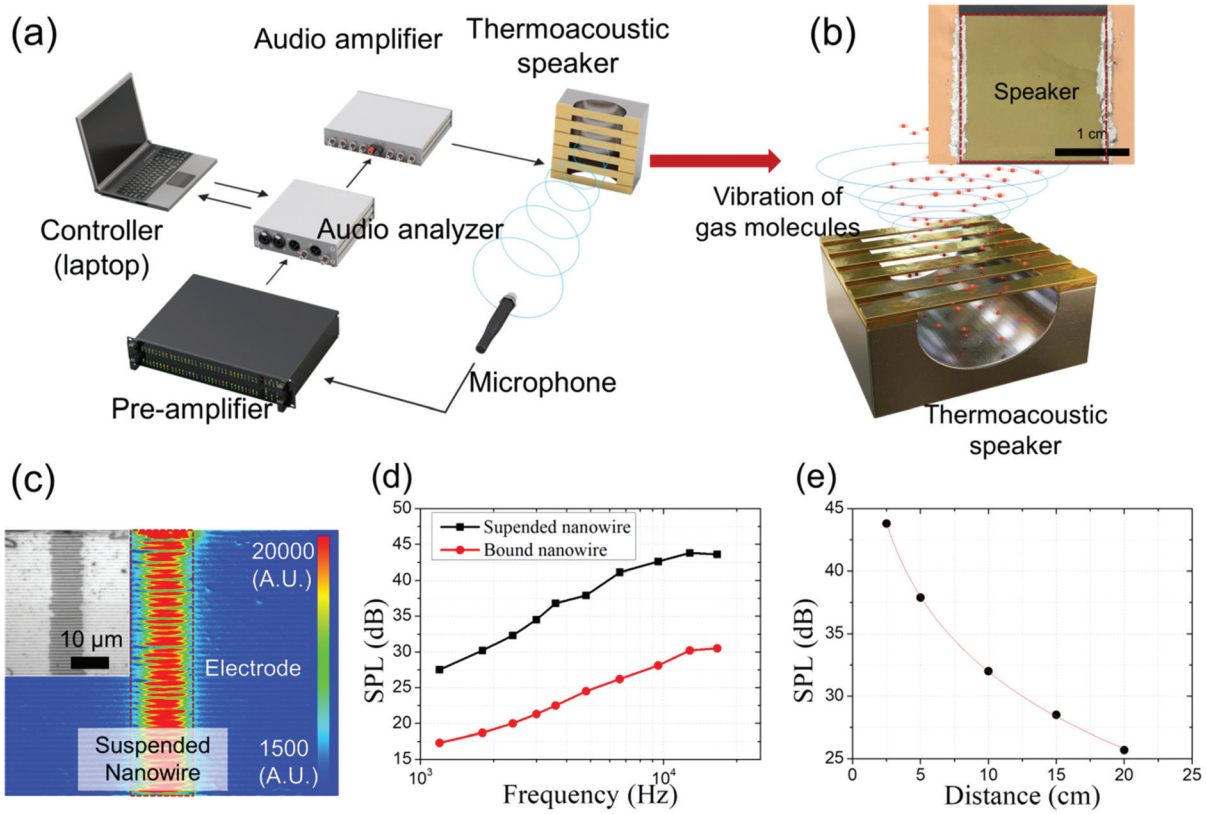


Fig. 4 Application of the suspended nanostructure to a thermoacoustic speaker. (a) Schematic of the experimental setup for characterizing the thermoacoustic speaker. (b) Schematic and photographic image of the fabricated thermoacoustic speaker. (c) Thermoreflectance microscopy image of the speaker under an applied voltage of 1.5 V. The inset image shows the enlarged microscopic image of the suspended region. The sound pressure level (SPL) of the speaker depending on (d) different frequencies under an applied power of 1 W and (e) measurement distance under an applied power of 1 W with a frequency of 4.8 kHz.

Similar to H_2 gas sensors, thermoacoustic speakers based on both conventional bound and suspended Au nanowire arrays have been fabricated. The fabricated speaker has Au nanowires (width = 600 nm) perpendicularly aligned on a periodic Au microline (width = 10 μm) array separated by dry-etched trenches (width = 10 μm, depth = 2 μm), as shown in Fig. 4b and Fig. S5.† Fig. 4c shows the relative temperature distribution of the suspended nanowires in the form of a thermoreflectance microscopy image. Notably, heat was generated only in the suspended nanowire region. This is attributed to the fact that the part where the Au microline and Au nanowires are welded has five times the electrical conductance of the suspended region, and the power consumed by Joule heating is inversely proportional to the electrical conductance in the series electrical circuit.[51] Through partial heating of the suspended region, it is possible to realize an efficient thermoacoustic speaker by minimizing the heat loss through the substrate. To evaluate the performance of each thermoacoustic speaker, the response characteristics of the speaker on the basis of the sound frequency were measured in an anechoic chamber, as shown in Fig. 4a and Fig. S6.† As shown in Fig. 4d, the suspended nanowire-based speaker has an approximately 20 dB higher sound pressure level (SPL) than the bound nanowire-based speaker at the same applied voltage input owing to the minimal influence of the substrate. In addition, the variation in the SPL depending on the measurement distance coincides with the theoretical logarithm function, as shown in Fig. 4e. Finally, three well-known classical songs were played using the suspended nanowire-based speaker: Mozart's *Turkish March*, Offenbach's *Can Can*, and Tchaikovsky's *Swan Lake Suite*, as demonstrated in Video S1.†

Conclusions

In summary, we demonstrated a rapid and simple method for fabricating wafer-scale, highly uniform, well-arrayed suspended nanostructures *via* nanowelding lithography. Because the rapid and parallel nanowelding lithography process requires only 3 min regardless of fabrication area, large-area suspended nanostructures could be effectively fabricated. In addition, various nanostructures (*e.g.*, nanowires, nanoholes, nanomesh, and nanofilms) and metals (*e.g.*, Au, Pd, and Ag) were chosen to fabricate the suspended nanostructures, which demonstrated the wide applicability of our method. As demonstrations, gas sensors and thermoacoustic speakers with well-

Published on 30 December 2021. Downloaded by Korea Advanced Institute of Science & Technology / KAIST on 11/21/2022 2:00:33 PM.

arrayed nanostructures were fabricated. Because the suspended nanostructure allows the devices to have a high SA : V and to minimize the influence of the substrate (*e.g.*, minimizing mechanical constraint for the gas sensor and minimizing heat loss for the thermoacoustic speaker), they outperformed those with unsuspended nanostructures. In future studies, the proposed suspended nanostructures fabricated *via* nanowelding technique can be utilized in several applications, such as photocatalysis, biosensors, and optical devices.

Author contributions

Z. J. Zhao and J. Ahn performed all experiments, analyzed the data, and wrote the paper. D. Lee, C. Jeong, M. Kang, J. Choi, M. Bok, S. Hwang, S. Jeon, S. Park, J. Ko, K. S. Chang, and J. W. Choi discussed the results. I. Park and J. H. Jeong led the overall direction of the project. All authors have given approval to the final version of the manuscript.

Conflicts of interest

There are no conflicts to declare.

Acknowledgements

This work was supported by the National Research Foundation of Korea (NRF) Grant funded by the Korean Government (MSIP) (No. 2021R1A2C3008742), the Center for Advanced Meta-Materials (CAMM) funded by the Ministry of Science, ICT and Future Planning, Korea, through the Global Frontier Project (CAMM-No. 2014M3A6B3063707), and Institute of Information & Communications Technology Planning & Evaluation (IITP) grant funded by the Korea government (MSIT) (No. 2020-0-00914, Development of hologram printing downsizing technology based on holographic optical element (HOE)).

Notes and references

1 M. Gao, M. Cho, H.-J. Han, Y. S. Jung and I. Park, *Small*, 2018, **14**, 1703691.
2 J. Seo, Y. Lim and H. Shin, *Sens. Actuators, B*, 2017, **247**, 564–572.
3 J. Ni, W. Wang, M. Quintana, F. Jia and S. Song, *Appl. Surf. Sci.*, 2020, **514**, 145911.
4 N. L. W. Septiani, A. G. Saputro, Y. V. Kaneti, A. L. Maulana, F. Fathurrahman, H. Lim, B. Yuliarto, Nugraha, H. K. Dipojono, D. Golberg and Y. Yamauchi, *ACS Appl. Nano Mater.*, 2020, **3**, 8982–8996.
5 S. Zhang, Q. Yang, X. Xu, X. Liu, Q. Li, J. Guo, N. L. Torad, S. M. Alshehri, T. Ahamad, M. S. A. Hossain, Y. V. Kaneti and Y. Yamauchi, *Nanoscale*, 2020, **29**, 15611–15619.
6 Y. V. Kaneti, N. L. W. Septiani, I. Saptiama, X. Jiang, B. Yuliarto, M. J. A. Shiddiky, N. Fukumitsu, Y.-M. Kang, D. Golberg and Y. Yamauchi, *J. Mater. Chem. A*, 2019, **7**, 3415–3425.
7 Z. Chen, Y. Wang, Y. Yang, X. Yang and X. Zhang, *Chem. Eng. J.*, 2021, **403**, 126388.
8 S. Mauthe, Y. Baumgartner, M. Sousa, Q. Ding, M. D. Rossell, A. Schenk, L. Czornomaz and K. E. Moselund, *Nat. Commun.*, 2020, **11**, 1.
9 S. Wang, P. C. Wu, V. C. Su, Y. C. Lai, M. K. Chen, H. Y. Kuo, B. H. Chen, Y. H. Chen, T. T. Huang, J. H. Wang, R. M. Lin, C. H. Kuan, T. Li, Z. Wang, S. Zhu and D. P. Tsai, *Nat. Nanotechnol.*, 2018, **13**, 227–232.
10 J. Ahn, Z. Zhao, J. Choi, Y. Jeong, S. Hwang, J. Ko, J. Gu, S. Jeon, J. Park, M. Kang, D. V. Del Orbe, I. Cho, H. Kang, M. Bok, J. Jeong and I. Park, *Nano Energy*, 2021, **85**, 105978.
11 Z. J. Zhao, J. Ahn, S. H. Hwang, J. Ko, Y. Jeong, M. Bok, H. J. Kang, J. Choi, S. Jeon, I. Park and J. H. Jeong, *ACS Nano*, 2021, **15**, 503–514.
12 D. Chen, P. Ning, Y. Zhang, J. Jing, M. Zhang, L. Zhang, J. Huang, X. He, T. Fu, Z. Song, G. He, D. Qian and X. Zhu, *ACS Appl. Mater. Interfaces*, 2020, **12**, 20138–20144.
13 A. P. Manuel, P. Barya, S. Riddell, S. Zeng, K. M. Alam and K. Shankar, *Nanotechnology*, 2020, **31**, 365301.
14 M. D. Levenson, N. S. Viswanathan and R. A. Simpson, *IEEE Trans. Electron Devices*, 1982, **29**, 1828–1836.
15 A. A. Tseng, K. Chen, C. D. Chen and K. J. Ma, *IEEE Trans. Electron. Packag. Manuf.*, 2003, **26**, 141–149.
16 L. J. Guo, *Adv. Mater.*, 2007, **19**, 495–513.
17 S. Lin, H. Wang, X. Zhang, D. Wang, D. Zu, J. Song, Z. Liu, Y. Huang, K. Huang, N. Tao, Z. Li, X. Bai, B. Li, M. Lei, Z. Yu and H. Wu, *Nano Energy*, 2019, **62**, 111–116.
18 A. Gans, E. Dressaire, B. Colnet, G. Saingier, M. Z. Bazant and A. Sauret, *Soft Mater.*, 2019, **15**, 252–261.
19 C. J. Brinker, Y. Lu, A. Sellinger and H. Fan, *Adv. Mater.*, 1999, **11**, 579–585.
20 D. H. Baek, J. Choi and J. Kim, *Sens. Actuators, B*, 2019, **284**, 362–368.
21 W. Fei, J. Zhou and W. Guo, *Small*, 2015, **11**, 2252–2256.
22 J. Lee, F. Ye, Z. Wang, R. Yang, J. Hu, Z. Mao, J. Wei and P. X.-L. Feng, *Nanoscale*, 2016, **8**, 7854–7860.
23 G. C. Gazzadi, S. Frabboni and C. Menozzi, *Nanotechnology*, 2007, **18**, 445709.
24 S. Heeg, R. Fernandez-Garcia, A. Oikonomou, F. Schedin, R. Narula, S. A. Maier, A. Vijayaraghavan and S. Reich, *Nano Lett.*, 2013, **13**, 301–308.
25 P. B. Agarwal, B. Alam, D. S. Sharma, S. Sharma, S. Mandal and A. Agarwal, *Flexible Printed Electron.*, 2018, **3**, 035001.
26 J. Choi and J. Kim, *Sens. Actuators, B*, 2009, **136**, 92–98.
27 Y. Lim, S. Kim, Y. M. Kwon, J. M. Baik and H. Shin, *Sens. Actuators, B*, 2018, **260**, 55–62.
28 J. Sim, K. Kim, S. Song and J. Kim, *Analyst*, 2013, **138**, 2432–2437.
29 D. Wang, X. He, J. Zhao, L. Jin and X. Ji, *IEEE Sens. J.*, 2020, **20**, 14646–14654.

 This journal is © The Royal Society of Chemistry 2022

Published on 30 December 2021. Downloaded by Korea Advanced Institute of Science & Technology / KAIST on 11/21/2022 2:00:33 PM.

30 K. Suzuki, S. Sakakibara, M. Okada, Y. Neo, H. Mimura, Y. Inoue and T. Murata, *Jpn. J. Appl. Phys.*, 2011, **50**, 01BJ10.
31 S. Kang, S. Cho, R. Shanker, H. Lee, J. Park, D. S. Um, Y. Lee and H. Ko, *Sci. Adv.*, 2018, **4**, eaas8772.
32 J. S. Lee, K. W. Choi, J. Y. Yoo, M. S. Jo and J. B. Yoon, *Small*, 2020, **16**, 1906845.
33 K.-W. Choi, M.-S. Jo, J.-S. Lee, J.-Y. Yoo and J.-B. Yoon, *Adv. Funct. Mater.*, 2020, **30**, 2004448.
34 Z. J. Zhao, S. H. Shin, D. G. Choi, S. H. Park and J. H. Jeong, *Small*, 2018, **14**, 29239109.
35 Z. J. Zhao, J. Ahn, J. Ko, Y. Jeong, M. Bok, S. H. Hwang, H. J. Kang, S. Jeon, J. Choi, I. Park and J. H. Jeong, *ACS Appl. Mater. Interfaces*, 2021, **13**, 3358–3368.
36 Occupational Safety and Health Administration (OSHA), *Toxic and Hazardous Substances*, Occupational Safety and Health Administration, DC, 2017, p. 1915.1000.
37 D. U. Kim, K. S. Park, C. B. Jeong, G. H. Kim and K. S. Chang, *Opt. Express*, 2016, **24**, 13906–13916.
38 D. U. Kim, J. D. Kim, I. Han, C. B. Jeong, K. Lee, H. Hur, K. Nam, J. Y. Bae, I. J. Kim and K. S. Chang, *IEEE Trans. Instrum. Meas.*, 2020, **69**, 2914–2923.
39 D. Sarkar, M. G. Baboly, M. M. Elahi, K. Abbas, J. Butner, D. Piñon, T. L. Ward, T. Hieber, A. Schuberth and Z. C. Leseman, *J. Micromech. Microeng.*, 2018, **28**, 045007.
40 I. Darmadi, F. A. A. Nugroho and C. Langhammer, *ACS Sens.*, 2020, **5**, 3306–3327.
41 M. Gao, M. Cho, Y. S. Jung and I. Park, *Small*, 2018, **14**, 1703691.
42 X. Q. Zeng, M. L. Latimer, Z. L. Xiao, S. Panuganti, U. Welp, W. K. Kwok and T. Xu, *Nano Lett.*, 2011, **11**, 262–268.
43 Z. J. Zhao, J. Ko, J. Ahn, M. Bok, M. Gao, S. H. Hwang, H. J. Kang, S. Jeon, I. Park and J. H. Jeong, *ACS Sens.*, 2020, **5**, 2367–2377.
44 M. Cho, J. Zhu, H. Kim, K. Kang and I. Park, *ACS Appl. Mater. Interfaces*, 2019, **11**, 13343–13349.
45 Y. Lim, Y. Lee, J.-I. Heo and H. Shin, *Sens. Actuators, B*, 2015, **210**, 218–224.
46 E. Lee, J. M. Lee, J. H. Koo, W. Lee and T. Lee, *Int. J. Hydrogen Energy*, 2010, **35**, 6984–6991.
47 F. Yang, D. K. Taggart and R. M. Penner, *Nano Lett.*, 2009, **9**, 2177–2182.
48 S. Kang, S. Cho, R. Shanker, H. Lee, J. Park, D. S. Um, Y. Lee and H. Ko, *Sci. Adv.*, 2018, **4**, eaas8772.
49 C. S. Kim, S. K. Hong, J. M. Lee, D. S. Kang, B. J. Cho and J. W. Choi, *Small*, 2016, **12**, 185–189.
50 A. O. Niskanen, J. Hassel, M. Tikander, P. Maijala, L. Grönberg and P. Helistö, *Appl. Phys. Lett.*, 2009, **95**, 163102.
51 J. Ahn, Y. Jeong, Z. Zhao, S. Hwang, K. Kim, J. Ko, S. Jeon, J. Park, H. Kang, J.-H. Jeong and I. Park, *Adv. Mater. Technol.*, 2020, **5**, 1900997.